Chapter 4

Native Oxide Films on AZ31 and AZ61 Commercial Magnesium Alloys – Corrosion Behaviour, Effect on Isothermal Oxidation and Sol–gel Thin Film Formation

Sebastián Feliu (Jr), Amir A. El Hadad,
Violeta Barranco, Irene Llorente,
Federico R. García-Galván,
Antonia Jiménez-Morales and Juan Carlos Galván

Additional information is available at the end of the chapter

http://dx.doi.org/10.5772/60721

Abstract

The authors present a review of their recent research work in an endeavour to interpret the influence of native oxide films on the corrosion behaviour of commercial AZ31 and AZ61 magnesium alloys or on the oxidation kinetics in air at 200°C. The tendency of some of these thin films to be sufficiently protective in mild or weak corrosive environments is examined. For obtaining oxide films with different protective properties, some of the specimens are tested with the surface in the as-received condition, while others are tested immediately after mechanical polishing. The technique applied to characterise thin (thickness of just a few nanometres) oxide films present on the surface of alloys has basically been XPS (X-ray photoelectron spectroscopy) in combination with ion sputtering. Oxidation resistance of the alloys is quantified by thermo gravimetric (TG) curves and their corrosion rate is evaluated by Electrochemical Impedance Spectroscopy (EIS) and hydrogen evolution measurement in chloride solutions with different aggressivity. Emphasis is placed on the possible effects of: (a) the different thickness of the native oxide films formed on the polished surfaces on the corrosion behaviour of the alloys; and (b) the different film homogeneity and uniformity on the oxidation results. Finally, an attempt will be made to learn more about the influence of the native oxide films that cover the substrate on the subsequent growth and protective behaviour of the sol–gel coatings.

Keywords: native oxide film, corrosion, magnesium alloys, surface chemistry, chloride, electrochemical impedance spectroscopy, x-ray photoelectron spectroscopy

1. Introduction

This chapter focuses on Mg–Al alloys, a material which has been transformed from a topic of scientific interest to a material of broad technological and commercial significance in the last two decades. From a practical point of view, Magnesium (Mg) is a promising structural material for transportation industries due to its low density (1.74 g/cm^3), high strength-to-weight ratio, good castability and mechanical properties, making it attractive for use in the automotive, aerospace and electronics industries, where light weighting is increasingly important. Especially for automotive industry, using lightweight materials like Mg can improve the fuel economy and have a positive impact on the emission of greenhouse gases and environment [1]. Unfortunately, magnesium and its alloys intrinsically have high chemical reactivity, which makes them susceptible to oxidation in various corrosive environments. The poor corrosion resistance of the magnesium alloy restricts its widespread application [2]. A better understanding of their corrosion mechanism, and of the factors influencing their corrosion behaviour, is expected to lead to more corrosion-resistant Mg alloys [3].

There are many scientific works that have studied the relationship between the microstructure of the alloy (quantity and distribution of the β-phase precipitates) or between Al content in the bulk of the alloys and their corrosion resistance [4-10]. Far fewer researchers have studied the chemical composition of the thin passivating layer on the outermost surface (thickness of about 3nm) which spontaneously grows in contact with the atmosphere or after short heat treatments at low temperature [11-15]. As it has been recently noted by Song [16], the rupture of an initially formed film can to a great extent influence the film growth behaviour in a later stage; the pitting distribution on a metal surface in an early stage will affect the final corrosion morphology; the initial surface cleanness of steel may sometimes determine the steel passivity. It is of great interest to learn how, when and where the transition suddenly starts. Predicting the occurrence of the transition on a metal surface is difficult, but it is a challenging goal that must be attained in corrosion research.

Like other metals, magnesium oxidises rapidly when exposed to the air or in an aqueous solution, giving rise to the formation of passivating oxide films of just a few nanometres thickness. According to Mott and Cabrera's theory on the growth of very thin oxide films [17], the electric field associated with the presence of oxygen ions adsorbed on the metal surface is enormous at first, but quickly weakens as the film thickness grows, and after a few minutes, the reaction virtually ceases. In dry air, at room temperature, the oxide reaches a limited thickness of about 4 nm, but can grow in thickness owing to the formation of magnesium hydroxide in a humid atmosphere and/or at a higher temperature.

http://dx.doi.org/10.5772/60721

From a scientific point of view, the literature contains controversial views relating to the effect of thin native oxide films characteristics on the corrosion performance of magnesium alloys. Chen et al. [18] reported that unlike other active light metals, such as Al and Ti, Mg alloys do not form a naturally passivating oxide film. In contrast, Nordlien et al. [19] and [20] and Lunder et al. [21] suggested that the oxide formed naturally on Mg–Al alloy surfaces is stable and protective and responsible for the passivity of the surface in the presence of an aqueous environment. Santamaria et al. [15] report that the films formed soon after mechanical treatment and immersion in aqueous electrolyte have a bilayer structure, consisting of an ultra-thin MgO inner layer (similar to 2.5 nm) and a $Mg(OH)_2$ external layer. Recently, Atrens et al. [22] proposed the partially protective surface film (PPSF) mechanism for Mg corrosion that assumes that the Mg surface is covered by a partially protective film, even in a concentrated chloride solution. However, the chemical composition and microstructure of the oxide films and their protection properties are still not clear [23].

According to Jeurgens et al. [24] and Saleh et al [25], the thermal oxidation of metallic alloys at low temperatures (e.g. at $T < 600$ K) and for short times has only scarcely been investigated. The detailed chemical composition and constitution of the oxide films formed on such alloy surfaces at low temperatures for short heating times are unknown. Furthermore, there is no comprehensive knowledge of the effect of the concurrent processes of chemical segregation and preferential oxidation on both the developing oxide-film microstructure and the induced compositional changes in the alloy subsurface.

Czerwinski [26] studied the oxidation behaviour of AZ91D Mg alloy at different temperatures. His results showed that AZ91D exhibited protective oxidation only at a temperature of 197°C, while at higher temperatures, the behaviour was non-protective and associated with the formation of oxide nodules and their coalescence into a loose fine-grained structure.

One of the main obstacles to characterise the thermally oxidised film formed on the surface of magnesium alloys after heating at low temperatures (200°C) is its small thickness. As Czerwinski [26] reported, the maximum oxide thickness achieved during heating (as converted from weight gain data) was equal to 64 nanometres for 197°C. This film thickness is too small to produce a sufficient signal for conventional materials characterisation techniques (Optical microscopy, SEM/EDX, XRD or TEM) [27]. The use of the XPS surface analysis technique makes it possible to reduce the analysed thickness to only 3 nm and supplies information on the oxidation state of the detected element.

One of the most effective ways to prevent corrosion of metals is to separate the metallic surface from the corrosive medium by mean of coating films. In this context, the sol-gel coatings have received considerable attention over the years, but recently there has been an upsurge of interest in these technologies due to the urgent necessity of searching an alternative way to the use of conventional primer coatings and pretreatments based in the use of Cr(VI) compounds. The great growth of the attention devoted to the sol-gel coatings is in part due to the new environmental protection legislation which restricts the use of chromium Cr(VI) salts because of their being highly toxic and carcinogenic. In the scientific literature, one can find valuable review papers that can be a good approach guide to understand the problems associated with the sol-gel science and technology [28-31].

The development of hybrid organic–inorganic sol-gel coating for protecting aircraft light alloys and improving environmentally benign surface treatments for aerospace alloys are topics of high priority around the world. In this way, Vreugdenhil et al. since 2001 described a process to develop Self-assembled NAnophase Particle (SNAP), which was based on the use of glycidylpropyltrimethoxysilane and tetramethylorthosilicate [32]. Afterwards, in 2003, these authors described a new route to improve the SNAP coating process. This new process was based on the use of amino-silanes as crosslinking agents 3-aminopropyltrimethoxysilane, 3-(2-aminoethyl) aminopropyltrimethoxysilane and 3-(trimethoxysilyl) propyldiethylenetriamine [33]. In a recent work, Li et al. have prepared a series of hybrid organic–inorganic coatings based on silica–epoxy composite coatings with the sol-gel method by using the amino-silane 3-aminopropyl triethoxysilane as a coupling agent and tetraethoxysilane to afford chemical bonding to form silica networks organic–inorganic hybrid coatings [34].

The production of hybrid sol-gel coatings is based in the co-hydrolysis and polycondensation of two organopolysiloxane precursors. One of them is the precursor of inorganic chain and another one is the former of the organic chain of the sol-gel network. Tetramethylorthosilicate and tetraethylorthosilicate are typically used as precursors of silica network [28-31]. On the other hand, aminopropyltrimethoxysilane, glycidylpropyltrimethoxysilane, methacryloyloxypropyltrimethoxysilane are commonly used as precursors of the organic chain. These molecules contain active groups that can react chemically with both the inorganic and organic substances, which can be used to design tailored multifunctional coatings with multiple properties (scratch, wear and corrosion resistance, superhydrophobicity, bioactivity and biocompatibility, environmentally benign antifouling, etc.) [28-31]. The use of mercapto silanes as the 3-mercaptopropyltrimethoxysilane can also be a good choice for preparing sol–gel coatings for light alloys [35].

Garcia Heras et al. have also prepared sol–gel coatings based on siloxane bonded units by starting from an organic–inorganic hybrid coatings by using as precursors γ-methacryloxypropyltrimethoxysilane and tetramethylorthosilicate for corrosion protection of zinc substrates Cerium nitrate hexahydrate in three different concentrations was added. The anticorrosive performance of the Ce^{3+} ions entrapped in the resulting hybrid silica sol–gel network occurs by means of the inhibitor effect and the self-healing mechanism (probably due to the $Ce(OH)_3$ precipitation) [36]. Recently, Harb et al. have reported a similar study where they also correlated the structural properties of cerium doped organic–inorganic hybrid coatings with their efficiency for the corrosion protection of carbon steel. The films were prepared via the sol–gel route from radical polymerisation of methyl methacrylate with 3-methacryloxy propyltrimethoxysilane followed by acidic hydrolysis and condensation of tetraethoxysilane [37]. A promising research line consists in introducing phosphorus precursors into organic–inorganic hybrid sol–gel coatings. In this way, El Hadad et al. have introduced triethylphosphite in sol–gel coatings based on mixtures of γ-methacryloxypropyltrimethoxysilane and tetramethylorthosilicate, not just for improving the corrosion protection properties of the coatings but also their biocompatibility [38].

Before, Khramov et al. had also used hybrid organic–inorganic coatings with phosphonate functionalities for evaluating their corrosion protection performance when they are used as

http://dx.doi.org/10.5772/60721

surface treatments for magnesium materials. These coatings have been processed via a sol–gel route by hydrolysis and condensation of a mixture of diethylphosphonatoethyltriethoxy-silane and tetraethoxy-silane obtaining very promising results [39]. In line with this idea, Lamaka et al. have synthesised hybrid organic–inorganic sols by copolymerisation of epoxy-siloxane and titanium or zirconium alkoxides by also using tris(trimethylsilyl) phosphate as additive to confer additional corrosion protection to magnesium-based alloy [40]. Barranco et al. have also evaluated the behaviour against corrosion of four optimised sol–gel coating systems (inorganic, hybrid organic–inorganic, containing zirconium and containing cerium ions) on magnesium alloys. These coatings were obtained by the sol–gel process from tetra-methoxysilane and diethoxydimethylsilane as organopolysiloxane precursors and were doped with Ce^{3+} to make evident their usefulness as autonomous protective coatings as well as a pretreatment prior to acrylic topcoat [41].To finish this section it might be interesting to mention a recent paper published by the group of Murillo-Gutierrez. These authors proposed the use of bilayer architectures as a strategy to improve the protection properties of sol–gel coatings on magnesium alloys. Because of the high reactivity of the magnesium alloys, a sol–gel coating based on a single layer presents defects consisting of macro-pores and protuberances, which opens access for corrosive species to reach the metallic substrate. This undesired effect can be overcome by using a sol–gel coating based on a bilayer architecture. For such a purpose, they use sol–gel formulations based on 3-glycidyloxypropyl-trimethoxysilane and aluminium-tri-sec-butoxide [42].

In this chapter, the authors present a review of their research work over the last three years on the correspondence between the chemical composition and physical characteristics of magnesium oxide layers present on the surface of commercial Mg–Al alloys and a series of metal properties including its microstructure, corrosion resistance, oxidation performance and sol–gel film formation. Most of the experimental information and results have been taken from published works by the authors [27, 43-47].

In the subsequent paragraphs, focused on the native oxide film, information is presented in relation with the following points:

1. Correspondence between thickness of the naturally formed oxide films on the surface of AZ31 and AZ61 alloys and a series of properties connected with the type of magnesium alloy, presence of second-phase particles in the magnesium matrix and the manufacturing conditions.
2. The corrosion resistance of the native oxide film in saline solutions of different aggressiveness.
3. The homogeneity and uniformity of the surface layer, which is closely related to the resistance by the magnesium alloys to the thermal oxidation.
4. The chemical changes in the native oxide surface film of the AZ61 alloy induced by the thermal oxidation at low temperatures and for short times, reinforcing its anticorrosive properties.
5. The behaviour of a silane hybrid sol–gel coating designed to be applied onto magnesium alloy surfaces for their corrosion protection.

2. Experimental section

Samples of wrought magnesium aluminium alloy (AZ31 or AZ61) in plates of 3 mm thickness were supplied by Magnesium Elektron Ltd, Manchester, UK. The chemical compositions of the tested magnesium alloys, AZ31 and AZ61, are listed in Table 1.

Alloy	Chemical Composition (wt%)						
	Al	Zn	Mn	Si	Fe	Ca	Mg
AZ31	3.1	0.73	0.25	0.02	0.005	0.0014	Balance
AZ61	6.2	0.74	0.23	0.04	0.004	0.0013	Balance

Table 1. Chemical composition of AZ31 and AZ61 alloys (wt%).

The following nomenclature is used in the remainder of the paper to designate the four dual combinations tested: AZ31-O, AZ31-P, AZ61-O and AZ61-P, where the letters O and P, which accompany the alloy type, denote: O= original surface condition (e.g. as-received condition); P= polished surface condition.

This research compares the behaviour of specimens of the above alloys in the following surface conditions:

Specimens in the as-received condition, where the untreated surfaces were only cleaned with distilled water and dried with hot air.

Freshly polished specimens were dry ground through successive grades of silicon carbide abrasive paper, from P600 to P2000, followed by finishing with 3 and 1 μm diamond paste, cleaned in distilled water and dried with hot air.

Two etching reagents were used: (a) nital 2%, 2 ml HNO_3 + 98 ml H_2O, to reveal the constituents and general microstructure of alloy AZ61 and (b) 4.6 g picric acid + 10 ml acetic acid + 70 ml ethanol + 10 ml H_2O to reveal the grain boundaries of alloy AZ31.

The thermal treatment was very simple, consisting of the horizontal exposure of 2 cm × 2 cm square specimens of the AZ31 and AZ61 alloys in a convective stove at 200 °C in air for 5, 20 and 60 min.

For preparation of sol–gel coatings, γ-methacryloxypropyltrimethoxysilane (MAPTMS) (98% from Aldrich) and tetramethoxysilane (TMOS) (98% from Fluka) have been used as received. Sols were prepared starting from a mixture of 4 mol of MAPTMS and 1 mol of TMOS. Ethanol and water were added with the molar ratio (TMOS + MAP)/water/ethanol of 1/7/8 [47]. The organic–inorganic hybrid coatings were deposited on the AZ31 and AZ61 by using a dip coating technique with a withdrawal speed of 9 cm/min and holding time of 60 s. The coated MAPTMS/TMOS-AZ31 alloy and MAPTMS/TMOS-AZ61 alloy systems were then placed in a furnace for 2 h at 120°C for curing. The rest of MAPTMS/TMOS sol was placed 12 h at 120 °C and crushed to convert it into a powder form [47].

AZ31 and AZ61 alloys were oxidised in identical conditions in a thermogravimetric analyser (TGA) (TA instruments Q600 SDT) using cylindrical specimens of 4 mm in diameter by 2 mm in height (weight approximately 100 mg). The apparatus was capable of accommodating a

http://dx.doi.org/10.5772/60721

specimen with a maximum weight of 0.5 g and had a measurement accuracy of 0.1 μg. The reaction temperature was monitored by a Pt/Pt–Rh thermocouple.

Weight change kinetics were measured in air under isothermal conditions at a temperature of 200 °C. The heating rate before reaching the isothermal condition was 50 °C/min.

The microstructure and chemical composition of the magnesium alloys were examined by the scanning electron microscopy (SEM, Hitachi S-4800) and by energy dispersive X-ray spectroscopy (EDS, Oxford energy dispersive X-ray microanalysis system) attached to SEM, respectively.

The surface topography of the specimens was measured ex situ by atomic force microscope (model 5100 AFM/SPM from Agilent Technologies) in taping mode with a resolution of 512 × 512 points.

Photoelectron spectra were recorded using a Fisons MT500 spectrometer equipped with a hemispherical electron analyser (CLAM 2) and an Mg Kα X-ray source operated at 300 W. The energies of all spectra were referenced to the C 1s peak at 285.0 eV. For acquiring the concentration profiles (distribution of elements as a function of specimen thickness), the surface was sputtered by argon ion bombardment (AIB) with a sputtering rate of 5 nm/min based on a SiO_2 reference. The data were analysed using a Xpspeak 4.1 software.

The morphology of the attack on the corroded surface was examined at low magnification and a camera was used to take the photographic images.

To measure the corrosion rate of magnesium alloys during immersion, hydrogen evolution detection tests were conducted at ambient temperature. The specimens were put in the beaker and then a funnel was located over the samples to collect the volume of evolved hydrogen during the corrosion process in a burette above the funnel.

Electrochemical impedance measurements were conducted in 0.006 M NaCl and 0.6 M NaCl at room temperature (25 °C). An AUTOLAB potentiostat, model PGSTAT30, with frequency response analyser (FRA) software was used. A three-electrode cell was used employing the magnesium alloy as working electrode with an exposed area of 1.0 cm^2, a graphite electrode as counter electrode and a saturated Ag/AgCl (saturated KCl) electrode as reference electrode, respectively. The impedance data were collected at the open circuit potential with a 10 mV sinusoidal AC perturbation over a frequency range of 100 kHz to 1 mHz. The Nyquist shapes of the completed experiments are fitted using the Zview program [48], and the impedance data are acquired from the fitting results using the equivalent electrical circuit.

3. Results and discussion

3.1. Characterisation of magnesium alloys

3.1.1. Morphology and structure of the outer oxide layer formed on AZ31 and AZ61 magnesium alloys with different surface conditions

Figure 1 compares the surface morphologies on the as-received (O) and polished (P) surface conditions for: (a, c) AZ31 alloy and (b, d) AZ61 alloy. As can be seen, the metallic surface of

the AZ31-O specimen appears to be covered by a large number of white precipitated particles (Figure 1a), whereas in the surface of the AZ61-O, these particles are not apparently visible (Figure 1b). In a previous study [45], we obtained EDX analyses on the white particles and an increase in the Al, Zn and Mn content and the decrease in the Mg content compared to the darker regions was observed. SEM examinations of the specimens in as-received condition (Figures 1a and 1b) revealed a rough surface covered with non-uniform features, very different to that of the polished surface (Figures 1c and 1d).

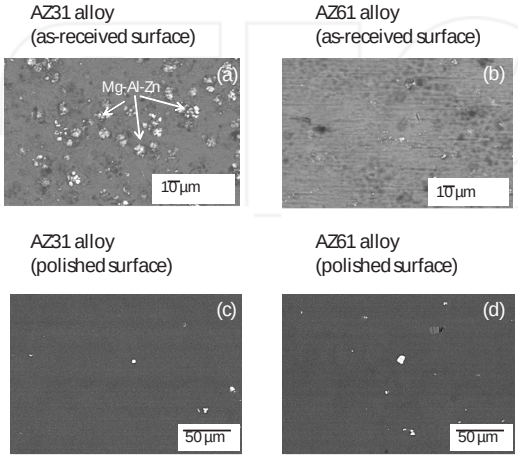

Figure 1. (a, b) SEM morphologies of the surfaces in the AZ31-O and AZ61-O and (c, d) AZ31-P and AZ61-P specimens (figure adapted from [45] and [46]).

Table 2 compares the surface roughness values on the AZ31-O and AZ61-O specimens with those corresponding to the AZ31-P and AZ61-P ones. Nanometric scale details of the typical surface roughness exhibited by the tested specimens are given in Figure 2.

SPECIMENS	RMS (nm)
AZ31-O	150.0
AZ61-O	138.6
AZ31-P	7.3
AZ61-P	5.6

Table 2. Roughness values obtained with atomic force microscope. The values are average of four determinations.

Figure 3 shows the SEM microstructure of the tested materials. Both alloys have an equiaxed grain structure typical of wrought magnesium alloys. The average grain sizes are approximately 5-100 μm (Figure 3a) and 40-100 μm (Figure 3b) in AZ31 and AZ61, respectively, but in AZ61 irregular-shaped divorced eutectic β-$Mg_{17}Al_{12}$ phases were seen at grain boundaries

http://dx.doi.org/10.5772/60721

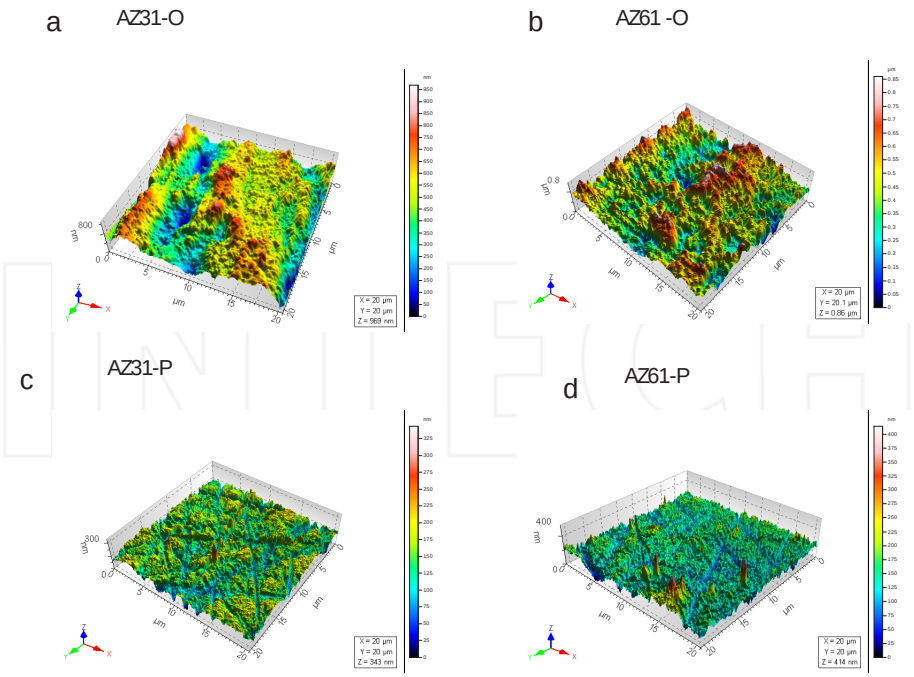

Figure 2. (a, b) Atomic-force Microscope (AFM) images of the surfaces in the AZ31-O and AZ61-O and (c, d) AZ31-P and AZ61-P specimens.

(Figure 3b). Microstructural features often promote the formation of points of attack on the surface of the specimens exposed to the test solution due to the discontinuities that are caused in the oxide film. In the case of AZ61, the small amounts of β-phase ($Mg_{17}Al_{12}$), which is formed at the grain boundaries (Figure 3b), can act as a galvanic cathode accelerating the corrosion of the α-Mg grain [49] and [50]. In contrast, it can be found that the alloying element Al in AZ31 alloy is completely dissolved into Mg matrix and no precipitation of β-phase is observed (Figure 3a). As will be seen later, the rate of corrosion is strongly influenced by the microstructure of the tested specimens.

3.1.2. Surface chemistry of the AZ31 and AZ61 magnesium alloys with different surface conditions

Figure 4 compares the C1s (a-d), O1s (e-h), Mg 2p (i-l) and Al 2s (m-p) XPS high-resolution spectra of the oxide films formed spontaneously on the surface of the AZ31 and AZ61 alloys after 5 minutes of sputtering. Attention is drawn to the absence of carbon on the surface of the specimens (Figures 4a-4d). The O 1s spectra (Figures 4e-4h) can be fitted to two components, which include the high binding energy component at 533.2 eV corresponding to the Al_2O_3 for the case of AZ31-P and AZ61-P specimens (Figures 4e and 4f), or $MgAl_2O_4$ for AZ31-O and AZ61-O specimens (Figures 4g and 4h) [51], and the low binding energy, most intense component at 531.2 eV relating the MgO [52].There are two components of similar intensity in

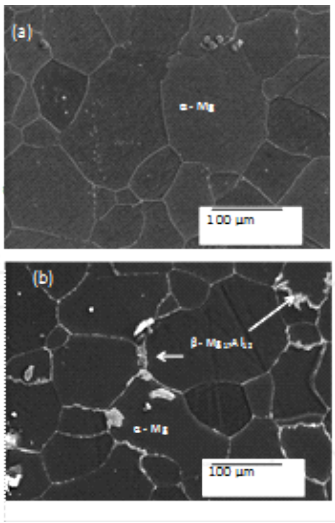

Figure 3. (a) SEM micrographs of AZ31 and (b) AZ61 magnesium alloys.

the Mg2p peak observed on the AZ31-P specimen (Figure 4i), in which the low binding energy component at 48.6 eV is attributed to metallic Mg, and the broader high binding energy peak centred at 50.8 eV corresponds to magnesium oxide (MgO). It can be seen that the ratio of the intensity of magnesium oxide component to the intensity of metallic magnesium component on the surface of the AZ61-P specimen (Figure 4j) is higher than on the AZ31-P specimen (Figure 4i). This is explained by accepting that the oxide film thickness on the AZ61-P specimen is greater. For AZ31-O and AZ61-O specimens (Figures 4k and 4l), the spectra are fairly similar, containing one single component at a binding energy of 50.8 eV associated with the presence of magnesium in the form of $MgAl_2O_4$ [51]. The Al2s spectra obtained on the AZ31-P, AZ31-O and AZ61-O specimens (Figures 4m, 4o and 4p) show a broad peak centred at 119.3–119.7 eV which indicates the presence of Al oxide and/or Al hydroxide. Attention is drawn to the presence of a significant metallic Al signal, which appears at approximately 117.3 eV, in the spectrum obtained on AZ61-P specimen (Figure 4n). The absence of a significant metallic aluminium signal on the AZ31-P, AZ31-O and AZ61-O specimens (Figures 4m, 4o and 4p) suggests that no appreciable quantities of Al^0 are located in the outer region of the material. In contrast, this aluminium is in metallic or free form on the surface layers of the AZ61-P specimen (Figure 4n).

The thickness of the native oxide film (d_o) on the surface of the magnesium specimens was calculated using the expression given by Strohmeier [53]

$$d_0(nm) = \lambda_{oxide} \sin\theta ln \frac{(I_{oxide}\ x\ \lambda_{metal}\ x\ N_{metal})}{(I_{metal}\ x\ \lambda_{oxide} x\ N_{oxide})} + 1 \quad (1)$$

http://dx.doi.org/10.5772/60721

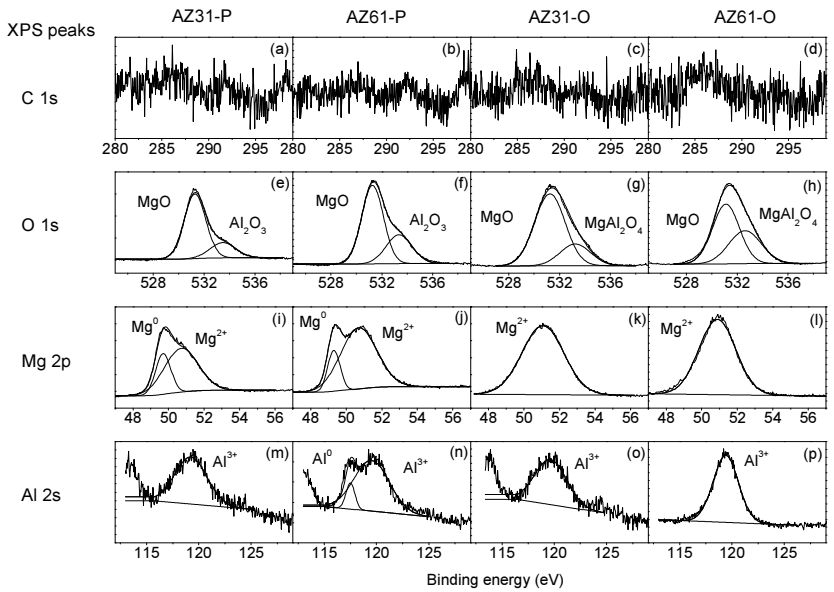

Figure 4. (a-d) Variation in the C1s, (e-h) O1s, (i-l) Mg2p and (m-p) Al2s high-resolution peaks obtained by XPS on the surface of the specimens after 5 min sputtering as a function of surface conditions and alloy type (figure adapted from [27]).

where I_{oxide} and I_{metal} denotes the component intensities, λ_{metal} and λ_{oxide} the mean free paths of photoelectrons of the metal atoms and the metal oxide, θ is the take-off angle for the analysed electrons, $\theta = 45°$ in this work; and N_{metal} and N_{oxide} correspond to the number density of the magnesium in metallic Mg and the surface layer. For the current investigation, an N_{metal}/N_{oxide} ratio of 1.24 was used [54]. The λ values for magnesium metal and magnesium oxide were kept as 3.0 and 2.6 nm [55-57], respectively. Figure 5 shows the oxide film thickness as calculated from Eq. (1) for the Mg2p peak after 3 min and 4.25 min (not shown), 5 min (Figures 4i and 4l) and 6 min of sputtering (not shown) in AZ31-P and AZ61-P specimens; and after 17 min, 20 min, 25 min and 30 min of sputtering (not shown) in AZ31-O and AZ61-O specimens. The thickness values have been determined by extrapolation to zero sputtering time.

From XPS analysis of oxide film thickness, it is observed that this value in the AZ61-P specimen is some 2 nm thicker than on the AZ31-P specimen (Figure 5a). The differences in film thickness among the two alloys are probably related with the degree of perfection of the oxide films and differences in diffusion rate of the reaction products [13], [26] and [58]. The higher film thickness values obtained with the AZ61 alloys, which contain more Al than AZ31 alloy, may be related to the heterogeneous structure associated with the β-precipitation phase located in the boundaries (Figure 3b). On the other hand, the presence of a coarse discontinuous outer layer of magnesium and aluminium oxides on the original surface of the AZ31-O and AZ61-O specimens (Figures 1a, 1b, 2a and 2b and Table 2) impedes the measurement of native oxide film thickness.

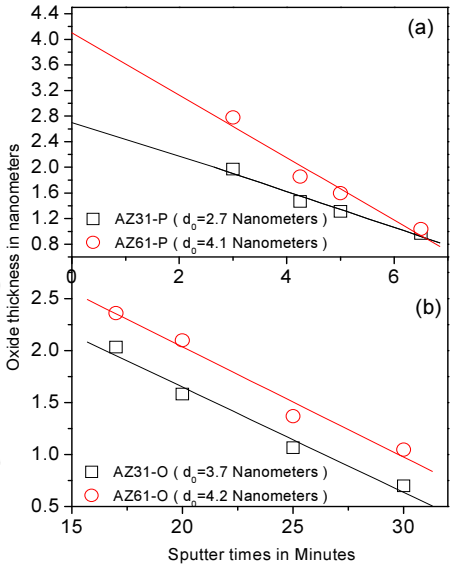

Figure 5. (a) Oxide thickness obtained by XPS on AZ31-P and AZ61-P specimens alloy and (b) in AZ31-O and AZ61-O specimens after sputtering (figure adapted from [27]).

3.2. Corrosion behaviour of magnesium alloys

The effect of native oxide films in chloride solutions at different times is described below.

3.2.1. Immersion tests

3.2.1.1. Hydrogen evolution measurements

Hydrogen evolution is dependent on the nature and composition of oxide films. Figure 6 shows the hydrogen evolution versus time curves (direct measure of the corrosion rate) during immersion in 0.006 M NaCl (a, d), 0.06 M NaCl (b, e) and 0.6 M NaCl (c, f) for 700 hours. No significant differences were observed in these curves for the AZ31-P specimen compared to the AZ31-O specimen, regardless the chloride concentrations of the solution (Figures 6a-6c). In contrast with the AZ31 alloy, significantly lower hydrogen evolution data were observed in the AZ61-P specimens during immersion in 0.006M (Figure 6d) and 0.06M NaCl (Figure 6e) than those corresponding to the AZ61-O substrate. Similar values of hydrogen volume evolved were measured in the AZ61-P specimen compared to those of the AZ61-O specimen during immersion in 0.6M NaCl (Figure 6f).

3.2.1.2. Electrochemical impedance measurements

The evolution of the corrosion process on the AZ31 and AZ61 alloys as a function of the surface conditions has been monitored by means of impedance measurements. It will be observed

http://dx.doi.org/10.5772/60721

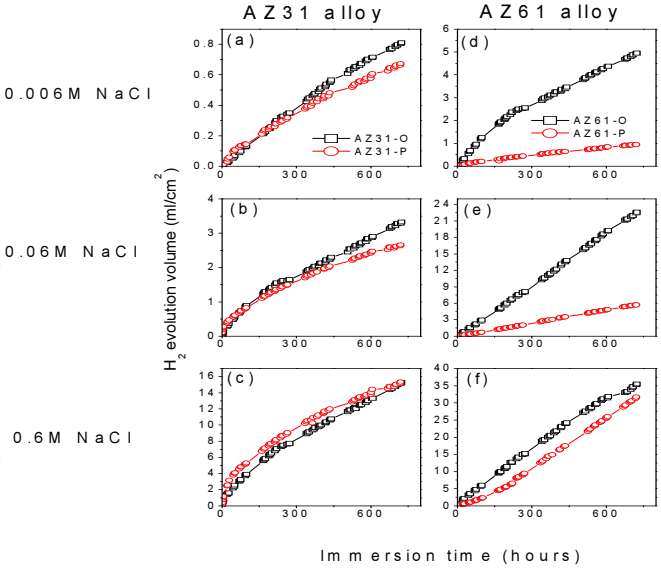

Figure 6. Comparison of the hydrogen evolution as a function of surface conditions and alloy type during 700 hours of immersion in saline solutions with different chloride ion concentrations.

from Figure 7 that all Nyquist diagrams exhibit a capacitive arc at high frequencies and intermediate frequencies (HF and MF) followed by an inductive arc in the low-frequency region (LF).

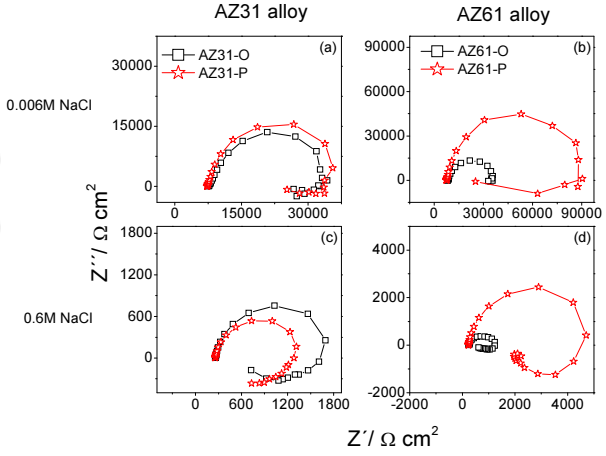

Figure 7. Comparison of the Nyquist plot as a function of substrate surface conditions and alloy type after 1 day of immersion in saline solutions with two different chloride ion concentrations.

In the literature about the corrosion of magnesium alloys, it is normal to associate the diameter of the capacitive loop in the HF/MF region with the charge transfer resistance (R_{CT}) of the corrosion process [9, 59, 60] value which is inversely related to the corrosion current (i_{corr}) through the well-known Stern-Geary equation [61]:

$$i_{corr} = \frac{B}{R_{CT}} \tag{2}$$

B being a proportionality constant which depends on the Tafel slopes, βa and βc. In this study, due to the uncertainty in the βa values from the polarisation curves [45], it was decided to use the constant B obtained empirically from the correlation between R_{CT} measurements and weight loss data [45]. Previous investigation [27] has justified the use of B values of 65 mV for the AZ31 alloy and 120 mV for the AZ61 alloy.

Table 3 compares the charge transfer resistance (R_{CT}) values for the AZ31 and AZ61 alloy specimens as a function of surface conditions and chloride ion concentration after one day of immersion. The corrosion current densities (mA/cm^2) obtained from Eq. (2) were converted to corrosion rates (mm/y) in Table 3 based on Faraday's law and the resulting equation:

$$corrosion\ rate\ =\ 22.85 i_{corr} \tag{3}$$

Specimens	Chloride ion concentration (M)	R_{CT} (Ω.cm^2)	Corrosion rate (mm/y)
AZ31-O	0.006	25000	0.06
AZ31-P		29000	0.05
AZ61-O		28000	0.10
AZ61-P		82000	0.03
AZ31-O	0.6	1500	1.0
AZ31-P		1100	1.3
AZ61-O		1000	2.7
AZ61-P		4000	0.7

Table 3. Variation in R_{CT} and corrosion rate values as a function of alloy-type surface condition and chloride ion concentration, after one day of immersion.

No significant differences in these values were observed in the AZ31-P specimen compared with those corresponding to the AZ31-O specimen (Table 3). In contrast with the AZ31 alloy, significantly lower corrosion rate values than the AZ61-O specimens were observed in those corresponding to the AZ61-P specimens (Table 3). It is interesting to note that similar trends regarding the corrosion behaviour are deduced from these electrochemical values as from the hydrogen evolution ones in 0.006 M NaCl (Figures 6a, d) and 0.06 M NaCl ones (Figures 6b, e).

http://dx.doi.org/10.5772/60721

The series of photographs in Figure 8 show that on the alloy AZ31 filiform corrosion is initiated almost immediately after immersion, especially on the AZ31-O specimen. The population of filaments expands in less than one day across the entire exposed surface. On the AZ61 alloy, the initiation and evolution of filiform corrosion is significantly slower than on AZ31, and clusters of propagating filaments do not appear until after 19 h of immersion on the as-received surface or 70 h on the polished surface. The small points in Figure 8 for AZ6-P specimen after 1 hour of immersion correspond to hydrogen bubbles growing at and detaching from the polished surface. In general, there is a qualitative agreement between the largest fraction of the corrosion area of the samples (Figure 8) and the electrochemical measurements (Table 3).

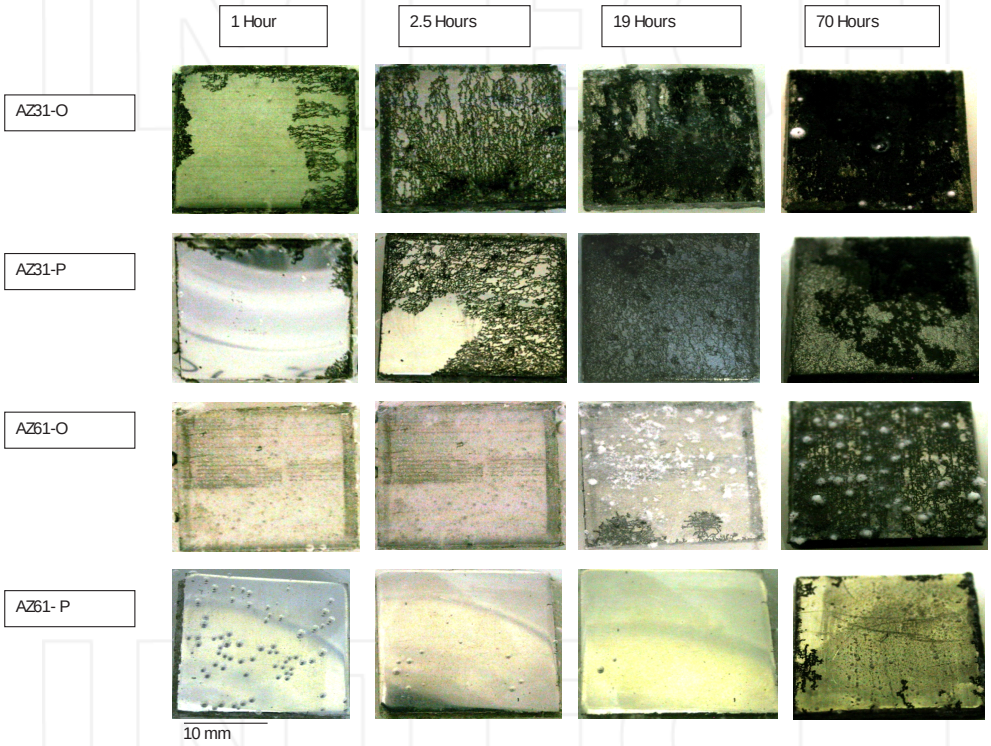

Figure 8. Photographic images of the evolution of corrosion morphology with immersion time for AZ31-O, AZ31-P, AZ61-O and AZ61-P specimens immersed horizontally about 50 mm below the surface of test solution (figure adapted from [44]).

As the results of the immersion tests, the native oxide film formed on the AZ31-P specimen does not reveal any particularly significant difference in corrosion resistance compared to those formed on the AZ31-O specimen (Figures 6a-c and Table 3).

Aluminium-rich particles containing high manganese, which are present in the alloy surface, can be detrimental to the corrosion resistance of Mg–Al alloys [62] The attack can be initiated

at points close to these particles which, acting as a galvanic cathode, accelerates alpha phase corrosion. In the present work, the presence of abundant white particles has been observed on the surface of the AZ31-O specimen (Figure 1a), while, these are practically irrelevant on the surface of the AZ31-P ones (Figure 1b). Curiously, the corrosion results in Figures 6a-c, Figures 7a, c and Table 3 reveal no special effect of the initial presence or absence of these particles on the surface of the AZ31 specimens.

In the immersion test in the 0.006 and 0.06 M NaCl, attention is drawn to the notably lower corrosion rate on the AZ61-P specimens compared to the AZ61-O specimens over 30 days testing (Figures 6d, e). This difference may be due to the strong protective effect of the oxide film that forms spontaneously on the polished AZ61 alloy surface, much more uniform, homogeneous and continuous than that on the as-received surfaces (Figures 1b, d, Figures 2b, d and Table 2). As long as these properties do not noticeably deteriorate with testing time, said film will prevent or slow the enhanced micro-galvanic action due to the abundant presence of β-phase in this alloy (Figure 3b) in posterior immersion in saline solutions of weak (0.006 M NaCl) or medium (0.06 M NaCl) aggressiveness.

One point emerging from the corrosion rate values in Table 3 is the clear trend of the AZ61-P specimen to present in the first day of immersion in presence of the highly aggressive 0.6 M NaCl solution lower values than the AZ31-P specimen. Also, this effect seems to be reflected in the series of photographs in Figure 8, where a large part of the surface of the AZ61-P specimen retains for a quite some time the initial shin, while soon the surface of the AZ31-P specimen appears affected by the corrosion. Comparing these results with the XPS determinations of oxide film thickness formed on the surface of the AZ61-P and AZ31-P specimens, one clearly see a tendency towards a decrease in corrosion rate values as the thickness of the spontaneously formed MgO film increases (Figure 5a). This correspondence between electrochemical values and the native oxide film thickness suggests that said film somehow controls the corrosive attack in the early stages of the immersion tests in the 0.6 M NaCl solution. It is logical to relate a decrease in the corrosion rate with the strengthening of the oxide film that usually protects the surface of magnesium alloys. Any increase in the native oxide film thickness decreases the percentage of active points or oxide-free areas on the metallic surface, inhibiting the tendency (stimulated by the presence of Cl- ions) for metallic ions to pass from the reactive bare surface into the aqueous solution. It is important to mention that, after an initial period which does not last for more than about 7 days, no effect attributable to the initial surface condition of the AZ61-P specimen is generally seen (Figure 6f).

3.3. Isothermal oxidation

There is the possibility that some of the more significant changes observed in the composition and specific characteristics of the metallic surface for the AZ31 and AZ61 alloys commented on previously, may exert an appreciable effect on the alloy oxidation kinetics at low temperatures. In this respect, attention is drawn to: (a) very thin MgO layer, only few nanometers thick, grown on the surface of AZ31-P and AZ61-P specimens; (b) the lack of continuity of the oxide film on the surface of AZ31-O and AZ61-O specimens resulting from the fabrication of the wrought alloy.

http://dx.doi.org/10.5772/60721

Figure 9 shows that the AZ31-P and AZ61-P specimens present much lower increases in weight gain during isothermal oxidation than the corresponding AZ31-O and AZ61-O specimens. As can be seen in Figure 9, 35–60 min of heating at 200 °C produces a very small weight gain, around only 0.6 μg/cm^2, which is similar for the two alloys. It is generally accepted that the growth of compact MgO films is controlled by solid-state diffusion through adherent oxide areas followed by the reaction with oxygen at the oxide/gas interface; hence, a lack of easy-paths for fast Mg transport could be a possible explanation for a highly protective behaviour [26]. From Eq. (4) [63]:

$$D_L = 1.0 \times 10^{-6} \exp\left(\frac{-150000}{RT}\right) \mathrm{m2/s} \quad (4)$$

Diffusivity (*DL*) of Mg within the MgO lattice at 473 K is as low as 2.67 × 10^{-23} m^2/s, justifying negligible weight gain.

This behaviour is not detected in the case of the AZ31-O and AZ61-O specimens (Figure 9), which tends to suggest that the increase in weight gain with the oxidation time is dependent on the initial surface condition of the studied alloys. As Table 2 shows, roughness values of the AZ31-O and AZ61-O specimens are more than ten times greater than for the AZ31-P and AZ61-P specimens. The difference in weight gain with heating time between the as-received and polished surfaces (Figure 9) may be in agreement with the very heterogeneous and likely defective surface layer present on the as-received surfaces (Figure 2) compared to the continuity of the oxide films formed on the polished specimens.

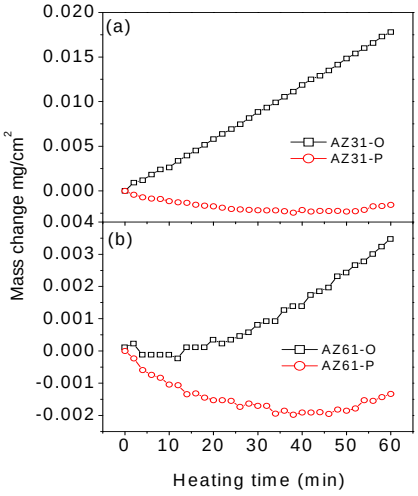

Figure 9. (a) Evolution of weight gain values obtained in the AZ31-O and (b) AZ61-O specimens as a function of the time of oxidation at 200°C in air compared with those of the same alloys in polished condition (figure adapted from [45]).

The evolution with sputtering time of the Al2s high-resolution XPS spectrum obtained on the oxide film formed on the surface of the AZ61-O and AZ61-P oxidised for 60 minutes in air at 200°C is shown in Figure 10. Attention is drawn to the high intensity of the Al^0 signal on the Al2s peak obtained on the AZ61-P specimen surface after 5 (Figure 10d) or 10 minutes of sputtering (Figure 10f) compared to its absence on the AZ61-O specimen surface (Figures 10c and 10e). This difference in trend suggests that a large part of the Al is in metallic state in the subsurface layers of the oxidised AZ61-P specimens, and as aluminium oxide or $MgAl_2O_4$ type species in the layers close to the outermost surface in the case of the heat-treated AZ61-O specimens. Jeurgens et al. [24] have investigated the growth kinetics and the evolution of the chemical composition and constitution of the initial oxide film grown on Mg-based MgAl surfaces by dry thermal oxidation, and observed that within the grown oxide films adjacent to the alloy/oxide interface, the interstitial sites were preferentially occupied by Al cations. In the present study, it is speculated that the homogeneous, uniform and compact native oxide layer present on the surface of the polished specimens (Figures 2c, d) inhibits significantly the oxidation or solid-state diffusion of the Al alloying element within the exposure times and temperature chosen in our study, inhibiting the growth of Al_2O_3 or $MgAl_2O_4$ type species [27].

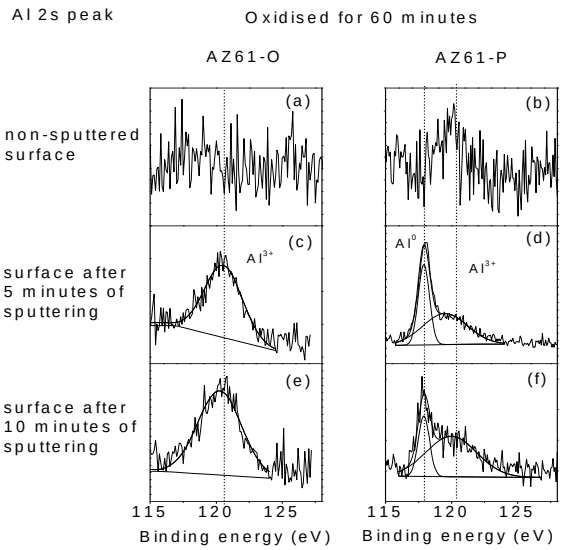

Figure 10. Variation of the Al2s high-resolution peak obtained by XPS on the surface of the AZ61-O and AZ61-P oxidised for 60 minutes as a function of the time of sputtering (figure adapted from [45] and [46]).

3.4. Native oxide film and sol–gel coating

In the XPS analysis of the external surface of the sol–gel coatings formed on the AZ31 substrate after the curing process, attention is drawn to the detection of significant amounts of magnesium (Table 4), which indicated the significant presence of discontinuities or pores in the

http://dx.doi.org/10.5772/60721

coating that leave the substrate surface exposed. In contrast, the absence of magnesium indicates that the surface of the AZ61 alloy substrate is completely covered by the sol–gel coating.

Alloy	%C	%O	%Si	%Mg
AZ31	16	53	29	2
AZ61	14	56	30	0

Table 4. Atomic percentage observed by XPS of the external surface of AZ31 and AZ61 coated with sol–gel.

Figures 11 and 12 display optical images and AFM topography images which represent the visual appearance and topography of the sol–gel coatings formed on the AZ31 substrate. It can be seen that the surface is not uniform, presenting areas without apparent defects coexisting with other areas with visible pores or defects. In contrast, the sol–gel coating formed on the AZ61 alloy substrate looks far more perfect and uniform (Figures 11 and 12). The formation of porous and non-uniform coatings during their deposition on magnesium alloys has been reported by Song and Liu [64]. This behaviour appears to be a result of the hydrogen evolution closely associated with the magnesium dissolution from the substrate.

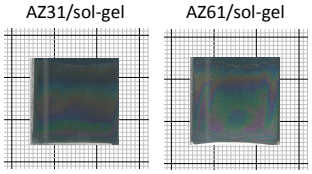

Figure 11. Optical pictures showing sol–gel coatings deposited on AZ31 and AZ61 magnesium alloy substrates.

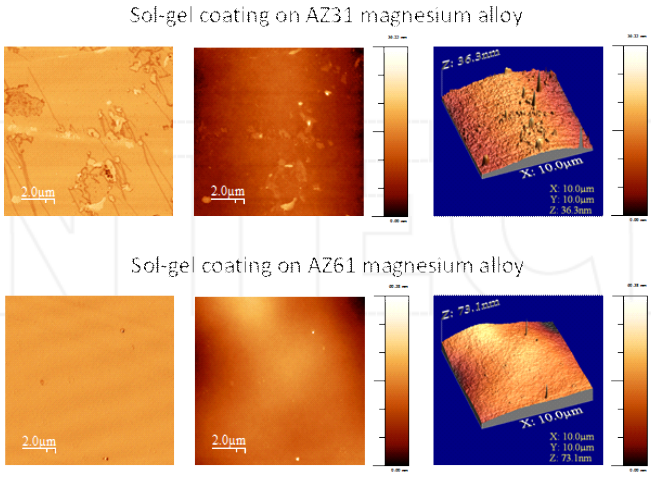

Figure 12. AFM topography images of the sol–gel coating formed on the AZ31 and AZ61 alloys substrates.

In previous studies [27], [43] and [44] with the same alloys immersed in a 0.6 M NaCl saline solution, we observed that the native oxide layer formed on the polished AZ61 surface was more protective than that on the AZ31 surface in the early stages of testing. The difference seemed to be due to the strong protective effect of the uniform, passive film of magnesium oxide that is formed spontaneously on the as-polished surface of the AZ61 magnesium alloy. At the beginning of the sol–gel coating formation, it is likely that this protective and homogeneous surface layer initially present on the polished AZ61 alloy substrate had a greater capability to isolate this alloy from the aqueous electrolyte environment and the effects of hydrogen evolution compared to the AZ31 alloy, resulting in the growth of a more perfect sol–gel coating than that of the AZ31 alloy.

It seems likely that some of the differences that have been revealed in the surface morphology of the sol–gel coatings formed on the AZ31 and AZ61 alloys have an impact on the corrosion behaviour. As commented earlier, the more significant changes that have been observed on the surface of the sol–gel coating, is the presence of defects or pores as a result of the interactions between coating and substrate during curing.

After less than 1 day of exposure, impedance measurements have revealed a significant reduction in the R_{HF} values of the coated AZ31 alloy substrate compared with those observed at the start of exposure (Figures 13 and 14). The presence of microscopic defects or pores in the coating formed on the AZ31 alloy (Figure 12) had the effect of decreasing its barrier properties, with any relevant influence on corrosion protection being lost.

In contrast to the findings with the AZ31 alloy, the sol–gel coating significantly improves the corrosion resistance of the AZ61 alloy as observed in the R_{HF} values obtained in the coated AZ61 samples, clearly exceeding the bare substrate values during the first seven days of corrosion testing in the presence of the highly aggressive 0.6 M NaCl solution (Figures 13 and 14). It seems likely that the uniformity and the absence of visible defects on the sol–gel coating formed on the AZ61 slow down the corrosion process by physically blocking the active sites on the metal surface (i.e. the presence of β-phase), diminishing the rate at which Cl^- ions are transported through the sol–gel coating.

The results obtained in this study show that the native oxide films spontaneously developed on AZ31 and AZ61 magnesium alloys prior coating exert a strong influence not just on the sol-gel thin film formation but also on the posterior corrosion protection behaviour of these sol–gel films when they are exposed to immersion tests to saline aqueous solutions. The chemical composition of the Mg–Al alloy is also a determinant factor to explain the subsequent growth of corrosion products on the metal substrates during immersion tests and the interactions of the corrosion products with the sol–gel films, exerting a remarkable effect on their posterior protection performance.

4. Conclusions

1. This chapter has summarised some of our work in an attempt to learn more about the influence of the native oxide films on the surface of AZ31 and AZ61 commercial magnesium alloys on their corrosion resistance in saline solutions of different aggressiveness.

http://dx.doi.org/10.5772/60721

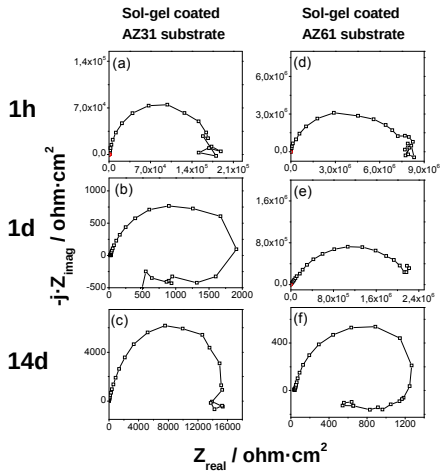

Figure 13. Variation in Nyquist plots as a function of the coated alloy-type substrate during immersion tests in 0.6 M NaCl aqueous solution.

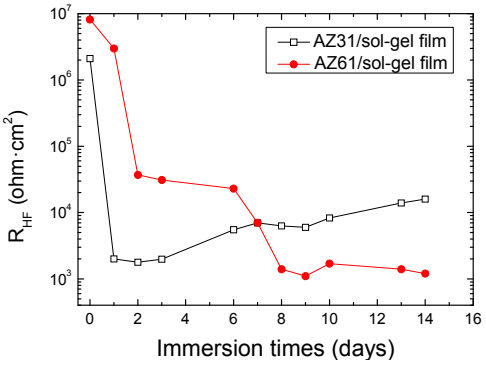

Figure 14. Variation in R_{HF} values as a function of the coated alloy-type substrate during immersion tests in 0.6 M NaCl aqueous solution.

2. The strong protective effect of the native oxide film that forms spontaneously on the polished AZ61 specimen, much more perfect and protective than the film on the as-received surface, prevents the fast micro-galvanic corrosion process present on the two-phase AZ61 alloy in weak or mild corrosive environments (0.006 M and 0.06 M NaCl solutions). In presence of the highly aggressive 0.6 M NaCl solution, the expected beneficial effect of the native oxide film has been shown in this investigation during the first hours or days of corrosion testing.

3. In contrast to the AZ61 alloy, it is important to mention that no effect attributable to the native oxide film is generally seen on the corrosion properties of the AZ31 alloy.

4. The results suggest some kind of link between the thickness of the native oxide film formed on the polished surfaces and the increase in the protective properties. From XPS determinations, it is found that the oxide film formed on the polished AZ61 alloy is some 1.4 nm thicker than on AZ31 alloy.

5. The difference in the isothermal oxidation behaviour at 200°C between the as-received and polished surfaces may be in agreement with the very heterogeneous and likely defective surface layer present on the as-received surfaces compared to the more uniform, homogeneous and continuous native oxide film formed on the polished surfaces. The native oxide layer present on the surface of the alloys inhibits significantly the oxidation or solid-state diffusion of the Al alloying element within the exposure times and temperature chosen in our study, reducing the adverse effects on the protective properties associated to the growth of Al_2O_3 or $MgAl_2O_4$ type species.

6. AFM, SEM and XPS analyses revealed that the sol–gel coatings formed on the surface of AZ61 alloy are far more perfect, uniform and free from microscopic defects than those formed on the AZ31 alloy. This behaviour is attributed to the effect of the native oxide film initially present on the surface of the AZ61 alloy, which inhibits the attack of magnesium. However, with the AZ31 alloy, the native oxide film is not sufficiently protective to prevent magnesium dissolution and associated hydrogen evolution, causing microscopic pores during the curing process of the sol–gel film formation.

Acknowledgements

The authors express their gratitude to Prof. S. Feliu for several clarifying and stimulating discussions during the course of this work. They also gratefully acknowledge financial support for this work from the Ministry of Economy and Competitivity of Spain (MAT 2009-13530 and MAT2012-30854).

Author details

Sebastián Feliu (Jr)[1*], Amir A. El Hadad[2], Violeta Barranco[3], Irene Llorente[1], Federico R. García-Galván[1], Antonia Jiménez-Morales[4] and Juan Carlos Galván[1]

*Address all correspondence to: sfeliu@cenim.csic.es

1 Centro Nacional de Investigaciones Metalúrgicas (CENIM), CSIC, Madrid, Spain

2 Physics Department, Faculty of Science, Al-Azhar University, Cairo, Egypt

3 Instituto de Ciencia de Materiales de Madrid (ICMM), CSIC, Madrid, Spain

4 Universidad Carlos III de Madrid, Departamento de Ciencia e Ingeniería de Materiales e Ingeniería Química, Leganés, Spain

http://dx.doi.org/10.5772/60721

References

[1] Wang C, Jiang B, Liu M, Ge Y. Corrosion characterization of micro-arc oxidization composite electrophoretic coating on AZ31B magnesium alloy. Journal of Alloys and Compounds 2015; 621(5) 53-61.

[2] Seifzadeh D, Bezaatpour A, Joghani RA. Corrosion inhibition effect of N, N'-bis (2-pyridylmethylidene)-1, 2-diiminoethane on AZ91D magnesium alloy in acidic media. Transactions of Nonferrous Metals Society of China 2014; 24(11) 3441-3451.

[3] Cao F, Shi Z, Song GL, Liu M, Dargusch M. Atrens A. Influence of casting porosity on the corrosion behaviour of Mg0.1Si. Corrosion Science. DOI:10.1016/j.corsci. 2015.02.002.

[4] Ballerini G, Bardi U, Bignucolo R, Ceraolo G. About some corrosion mechanisms of AZ91D magnesium alloy. Corrosion Science 2005; 47(9) 2173-2184.

[5] Song GL, Atrens A, Wu XL, Zhang B. Corrosion behaviour of AZ21, AZ501 and AZ91 in sodium chloride. Corrosion Science 1998; 40(10) 1769-1791.

[6] Song GL, Atrens A, Dargusch M. Influence of microstructure on the corrosion of diecast AZ91D. Corrosion Science 1999; 41(2) 249-273.

[7] Ambat R, Aung NN, Zhou W. Evaluation of microstructural effects on corrosion behaviour of AZ91D magnesium alloy. Corrosion Science 2000; 42(8) 1433-1455.

[8] Song GL, Atrens A. Corrosion mechanisms of magnesium alloys. Advanced Engineering Materials 1999; 1(1) 11–33.

[9] Mathieu S, Rapin C, Hazan J, Steinmetz P. Corrosion behaviour of high pressure diecast and semi-solid cast AZ91D alloys. Corrosion Science 2002; 44(12) 2737–2756.

[10] Galicia G, Pebere N, Tribollet B, Vivier V. Local and global electrochemical impedances applied to the corrosion behaviour of an AZ91 magnesium alloy. Corrosion Science 2009; 51(8) 1789-1794.

[11] Fournier V, Marcus P, Olefjord I. Oxidation of magnesium. Surface and Interface Analysis 2002; 34(1) 494-497.

[12] Fotea C, Callaway J, Alexander MR. Characterisation of the surface chemistry of magnesium exposed to the ambient atmosphere. Surface and Interface Analysis 2006; 38(10) 1363-1371.

[13] McIntyre NS, Chen C, Role of impurities on Mg surfaces under ambient exposure conditions. Corrosion Science 1998; 40(10) 1697-1709.

[14] Chen C, Splinter SJ, Do T, McIntyre NS. Measurement of oxide film growth on Mg and Al surfaces over extended periods using XPS. Surface Science 1997; 382 (1-3) L652-L657.

[15] Santamaria M, Di Quarto F, Zanna S, Marcus P. Initial surface film on magnesium metal: A characterization by X-ray photoelectron spectroscopy (XPS) and photocurrent spectroscopy (PCS). Electrochimica. Acta 2007; 53(3) 1314-1324.

[16] Song GL. The grand challenges in electrochemical corrosion research. Frontiers in Materials 2014; DOI: 10.3389/fmats.2014.00002.

[17] Cabrera N, Mott NF. Theory of the oxidation of metals. Reports on Progress in Physics 1948; 12 163-184.

[18] Chen XB, Birbilis N, Abbott TB. Review of corrosion-resistant conversion coatings for magnesium and its alloys. Corrosion 2011; 67(3) Article Number: 035005.

[19] Nordlien JH, Nisancioglu K, Ono S, Masuko N. Morphology and structure of oxide films formed on MgAl alloys by exposure to air and water. Journal of the Electrochemical Society 1996; 143(8) 2564-2572.

[20] Nordlien JH, Nisancioglu K, Ono S, Masuko N. Morphology and structure of water-formed oxides on ternary MgAl alloys. Journal of the Electrochemical Society 1997; 144(2) 461-466.

[21] Lunder O, Lein JE, Aune TK, Nisancioglu K. The role of Mg17Al12 phase in the corrosion of Mg alloy AZ91. Corrosion 1989; 45(9) 741-748.

[22] Atrens A, Song GL, Cao F, Shi Z, Bowen PK. Advances in Mg corrosion and research suggestions. Journal of Magnesium and Alloys 2013; 1(3) 177-200.

[23] Song YW, Han EH, Dong KH, Shan DY, Yim CD, You BS. Study of the corrosion product films formed on the surface of Mg–xZn alloys in NaCl solution. Corrosion Science 2014; 88 215-225.

[24] Jeurgens LPH, Vinodh MS, Mittemeijer EJ. Initial oxide-film growth on Mg-based MgAl alloys at room temperature. Acta Materialia 2008; 56(17) 4621-4634.

[25] Saleh H, Weling T, Seidel J, Schmidtchen M, Kawalla R, Mertens FORL, Vogt HP. An XPS study of native oxide and isothermal oxidation kinetics at 300°C of AZ31 twin roll cast magnesium alloy. Oxidation of Metals 2014; 81(5-6) 529-548.

[26] Czerwinski F. The oxidation behaviour of an AZ91D magnesium alloy at high temperatures. Acta Materialia 2002; 50(10) 2639-2654.

[27] Feliu Jr. S, Maffiotte C, Samaniego A, Galván JC, Barranco V. Effect of the chemistry and structure of the native oxide surface film on the corrosion properties of commercial AZ31 and AZ61 alloys. Applied Surface Science 2011; 257(20) 8558-8568.

[28] Zheludkevich ML, Salvado IM, Ferreira MGS. Sol-gel coatings for corrosion protection of metals. Journal of Materials Chemistry 2005; 15(48) 5099-5111.

[29] Wang D, Bierwagen G R. Sol-gel coatings on metals for corrosion protection. Progress in Organic Coatings 2009; 64 (4) 327-338.

http://dx.doi.org/10.5772/60721

[30] Zheng SX, Li JH. Inorganic-organic sol gel hybrid coatings for corrosion protection of metals. Journal of Sol-Gel Science and Technology 2010; 54(2)174-187.

[31] Figueira RB, Silva CJR, Pereira EV. Organic–inorganic hybrid sol–gel coatings for metal corrosion protection: a review of recent progress. Journal of Coatings Technology Research 2015; 12(1) 1-35.

[32] Vreugdenhil AJ, Balbyshev VN, Donley MS. Nanostructured silicon sol-gel surface treatments for Al 2024-T3 protection. Journal of Coatings Technology 2001; 73(915) 35-43.

[33] Khramov AN, Balbyshev VN, Voevodin NN, Donley MS. Nanostructured sol-gel derived conversion coatings based on epoxy- and amino-silanes. Progress in Organic Coatings 2003; 47(3–4) 207–213.

[34] Li WL, Huang D, Xing XY, Tang JJ, Xing YJ, Li XJ, Zhang JD. Study the factors affecting the performance of organic-inorganic hybrid coatings. Journal of Applied Polymer Science 2014; 131(21) 41010.

[35] Vignesh RB, Edison TNJI, Sethuraman MG. Sol–gel coating with 3-mercaptopropyltrimethoxysilane as precursor for corrosion protection of aluminium metal. Journal of Materials Science & Technology 2014; 30 (8) 814–820.

[36] Garcia-Heras M, Jimenez-Morales A, Casal B, Galvan JC, Radzki S, Villegas MA. Preparation and electrochemical study of cerium-silica sol-gel thin films. Journal of Alloys and Compounds 2004; 380 (1-2) 219-224.

[37] Harb SV, Santos FCD, Caetano BL, Pulcinelli SH, Santilli CV, Hammer P. Structural properties of cerium doped siloxane-PMMA hybrid coatings with high anticorrosive performance. RSC Advances 2015; 5 (20) 15414-15424.

[38] El Hadad AA, Barranco V, Jiménez-Morales A, Hickman GJ, Galván JC, Perry, CC. Triethylphosphite as a network forming agent enhances in vitro biocompatibility and corrosion protection of hybrid organic-inorganic sol-gel coatings for Ti6Al4V alloys. Journal of Materials Chemistry B 2014; 2 (45) 7955-7963.

[39] Khramov AN, Balbyshev VN, Kasten LS, Mantz RA. Sol-gel coatings with phosphonate functionalities for surface modification of magnesium alloys. Thin Solid Films 2006; 514 (1-2) 174-181.

[40] Lamaka SV, Montemor MF, Galio AF, Zheludkevich ML, Trindade C, Dick LF, Ferreira MGS. Novel hybrid sol-gel coatings for corrosion protection of AZ31B magnesium alloy. Electrochimica Acta 2008; 53 (14) 4773-4783.

[41] Barranco V, Carmona N, Galván JC, Grobelny M, Kwiatowski L. Electrochemical study of tailored sol-gel thin films as pre-treatment prior to organic coating for AZ91 magnesium alloy. Progress in Organic Coatings 2010; 68(4) 347-355.

[42] Murillo-Gutiérrez NV, Ansart F, Bonino JP, Kunst SR, Malfatti CF. Architectural optimization of an epoxy-based hybrid sol-gel coating for the corrosion protection of a cast Elektron21 magnesium alloy. Applied Surface Science 2014; 309 62-73.

[43] Feliu Jr. S, Maffiotte C, Samaniego A, Galvan JC, Barranco V. Effect of naturally formed oxide films and other variables in the early stages of Mg-alloy corrosion in NaCl solution. Electrochimica Acta 2011; 56(12) 4454-4565.

[44] Samaniego A, Llorente I, Feliu Jr. S. Combined effect of composition and surface condition on corrosion behaviour of magnesium alloys AZ31 and AZ61. Corrosion Science 2013; 68 66-71.

[45] Feliu Jr. S, Samaniego A, Barranco V, El-Hadad AA, Llorente I, Adeva P. The effect of low temperature heat treatment on surface chemistry and corrosion resistance of commercial magnesium alloys AZ31 and AZ61 in 0.6 M NaCl solution. Corrosion Science 2014; 80 461-472.

[46] Feliu Jr. S, Samaniego A, Barranco V, El-Hadad AA, Llorente I, Serra C, Galvan JC. A study on the relationships between corrosion properties and chemistry of thermally oxidised surface films formed on polished commercial magnesium alloys AZ31 and AZ61. Applied Surface Science 2014; 295 219-230.

[47] El-Hadad AA, Barranco V, Samaniego A, Llorente I, García-Galván FR, Jímenez-Morales A, Galván JC, Feliu Jr. S. Influence of substrate composition on corrosion protection of sol–gel thin films on magnesium alloys in 0.6 M NaCl aqueous solution. Progress in Organic Coatings 2014; 77(11) 1642-1652.

[48] ZView Software, Version 3.1c; Scribner Associates Inc.: Southern Pines, NC, USA, 2007.

[49] Song GL, Atrens A. Understanding magnesium corrosion – a framework for improved alloy performance. Advanced Engineering Materials 2003; 5(12) 837–858.

[50] Liu M, Schmutz P, Uggowitzer PJ, Song GL, Atrens A. The influence of yttrium (Y) on the corrosion of Mg–Y binary alloys. Corrosion Science 2010; 52(11) 3687–3701.

[51] Feliu Jr. S, Maffiotte C, Galván JC, Pardo A, Merino MC, Arrabal R. The application of X-ray photoelectron spectroscopy in understanding corrosion mechanisms of magnesium and Mg-Al Alloys. The Open Surface Science Journal 2011; 3 1-14.

[52] Kim J, Wong KC, Wong PC, Kulinich SA, Metson JB, Mitchell KAR. Characterization of AZ91 magnesium alloy and organosilane adsorption on its surface. Applied Surface Science 2007; 253(9) 4197-4207.

[53] Strohmeier BR. An ESCA method for determining the oxide thickness on aluminium-alloys. Surface and Interface Analysis 1990; 15(1) 51-56.

[54] Liu M, Zanna S, Ardelean H, Frateur I, Schmutz P, Song GL, Atrens A, Marcus P. A first quantitative XPS study of the surface films formed, by exposure to water, on Mg

and on the Mg–Al intermetallics: Al3Mg2 and Mg17Al12. Corrosion Science 2009; 51(5) 1115-1127.

[55] Tanuma S, Powell CJ, Penn DR. Calculations of electron inelastic mean free paths. 2. Data for 27 elements over the 50–2000 eV range. Surface and Interface Analysis 1991; 17(13) 911-926.

[56] Akkerman A, Boutboul T, Breskin A, Chechik R, Gibrekhterman A, Lifshitz Y. Inelastic electron interactions in the energy range 50 eV to 10 keV in insulators: alkali halides and metal oxides. Physica Status Solidi (b) 1996; 198(2) 769-784.

[57] Powell CJ, Jablonski A. NIST electron inelastic-mean-free-path database, SRD 71, US Department of Commerce National Institute of Standards and Technology, Gaithersburg, MD, 2000.

[58] Feliu Jr. S, Bartolomé MJ. Influence of alloying elements and etching treatment on the passivating films formed on aluminium alloys. Surface and Interface Analysis 2007; 39(4) 304-316.

[59] Pebere N, Riera C, Dabosi F. Investigation of magnesium corrosion in aerated sodium-sulfate solution by electrochemical impedance spectroscopy. Electrochimica Acta 1990; 35(2) 555-561.

[60] Makar L, Kruger J. Corrosion studies of rapidly solidified magnesium alloys. Journal of the Electrochemical Society 1990; 137(2) 414-421.

[61] Stern M, Geary AL. Electrochemical polarization 1. A theoretical analysis of the shape of polarization curves. Journal of the Electrochemical Society 1957; 104(1) 56-63.

[62] Zeng R, Zhang J, Huang W, Dietzel W, Kainer KU, Blawert C, Ke W. Review of studies on corrosion of magnesium alloys. Transactions of Nonferrous Metals Society of China. 2006;16(1) s763-s771.

[63] Lea C, Molinari C. Magnesium diffusion, surface segregation and oxidation in Al–Mg alloys. Journal of Materials Science 1984; 19(7) 2336-2352.

[64] Song GL, Liu MH. The effect of Mg alloy substrate on "electroless" E-coating performance. Corrosion Science 2011; 53(11) 3500-3508.